Interface roughness evolution in sputtered WSi_2/Si multilayers

Yi-Ping Wang, Hua Zhou, Lan Zhou, and Randall L. Headrick[a)]
Department of Physics, University of Vermont, Burlington, Vermont 05405

Albert T. Macrander
Advanced Photon Source, Argonne National Laboratory, Argonne, Illinois 60439

Ahmet S. Özcan
Department of Physics, Boston University, Boston, Massachusetts 02215

(Received 15 July 2006; accepted 5 November 2006; published online 16 January 2007)

We report on the growth of WSi_2 and Si amorphous thin films by dc magnetron sputtering. *In situ* synchrotron x-ray scattering with high temporal resolution has been employed to probe the surface and interface roughness during film deposition. It is found that the WSi_2/Si multilayer surface alternately roughens and smoothes during deposition; while the Si layer roughness monotonically, the WSi_2 layer is observed to smooth out when deposited on an initially rough surface. Subsequent deposition of the next layer effectively freezes in the surface morphology of the previous layer in each case. Energetic neutrals and ions assisting the growth may play a role in inducing this pronounced alternating pattern in the roughness. © *2007 American Institute of Physics*.
[DOI: 10.1063/1.2422713]

I. INTRODUCTION

Amorphous multilayers have many applications in x-ray optical devices for x-ray microscopy, x-ray astronomy, x-ray lithography, and x-ray microanalysis. Many of these devices require reduced interface roughness in order to approach their optimum theoretical performance.[1–6] In this article, we discuss results for the WSi_2/Si bilayer system, which has been the system chosen in recent efforts to produce x-ray Laue focusing lenses with nanometer-scale line or point focus.[7,8]

The roughness evolution of both single layer and multilayer films deposited by sputter deposition has been intensively investigated.[9–16] In general, for a single amorphous layer grown on a flat substrate, shot noise is considered to be the main roughening mechanism during thin film deposition. Ultimately, surface roughness is a result of competition between smoothing effects and the shot noise driven roughening effect. In the early stages of thin film growth, the roughness amplitude is often found to increase monotonically, following a scaling behavior $R \sim t^{\beta}$, where t is deposition time and β is the growth exponent.[9,17,18] In sputter deposition, energetic particles may cause either roughening or smoothing, and are a by-product of the sputtering of the primary target material. However, the role of the energetic particles on the smoothing mechanisms in the sputtering process is still not very clear.

Previous studies carried out on Mo/Si multilayers have exhibited reduced roughness at lower working pressure.[4,5] A smoothing effect is inferred, which is explained in terms of energetic particle bombardment of the surface: the decreased gas pressure results in fewer collisions between the incident particles and the sputtering gas so that the deposited atoms and other particles are not thermalized. The higher average energy results in increased surface relaxation, which in turn, leads to smoothing of high-frequency roughness. Several mechanisms have been proposed, which may be responsible for the smoothing. For example, smoothing by viscous flow of amorphous materials was demonstrated as a result of ion bombardment on SiO_2.[19,20] Moseler *et al.* have suggested that smoothing by impact-induced downhill currents produces smoothing on any amorphous material.[13] It has also been demonstrated that an ion-beam-assisted sputter deposition process, known as ion polishing, can produce multilayers with reduced interface roughness.[2,16,21,22]

On the other hand, the energetic particles present in the sputter deposition process are often regarded as a disadvantageous factor that will lead to interface mixing.[2,6] It is believed that intermixing induced by energetic target atoms results in an asymmetrical interface roughness structure.[6] High-Z target materials produce more energetic particles during sputter deposition, particularly back reflected argon neutrals.[23] Since these energetic particles are expected to produce interface mixing, this idea can possibly explain an observed alternating rough/smooth interface morphology when the interface with the high-Z element on top is rougher than the light-over-heavy interface.

In this paper, we have used *in situ* real-time synchrotron x-ray scattering to investigate the roughness evolution in sputtered WSi_2 and Si single layers and WSi_2/Si multilayers. The specular reflection intensity of a thin film as a function of the deposited thickness can be described by the kinematical approximation

$$I = \left| \left(\frac{\rho_{\mathrm{sub}} - \rho_{\mathrm{film}}}{\rho_{\mathrm{sub}}} \right) e^{-Q^2 \sigma_{\mathrm{sub}}^2} + \frac{\rho_{\mathrm{film}}}{\rho_{\mathrm{sub}}} e^{-Q^2 \sigma_{\mathrm{film}}^2} e^{iQd} \right|^2 I_F, \qquad (1)$$

where I is the specular reflection intensity from the thin film and I_F is the Fresnel reflection intensity of the substrate.[24] The reflectivity also depends on the electron density of the thin film, ρ_{film}, the electron density of the substrate, ρ_{sub}, the

[a)]Electronic mail: rheadrick@uvm.edu

thickness of the film, d, and the roughness of the film and substrate, σ_{film} and σ_{sub}, respectively. The momentum transfer is $Q=2k\sin(\alpha_i)$, where k is the wave vector of x ray and α_i is the incident angle. According to the equation, the reflection intensity of the film will oscillate periodically with the thin film thickness, and the oscillation amplitude is determined by surface roughness. If surface roughness increases rapidly during film growth, the oscillations will quickly damp out and no oscillation can be observed when the film is beyond a certain roughness. We note that Eq. (1) can also be straightforwardly extended to the situation of multilayers.[24]

One of the main goals of this study is to determine whether the ion mixing and surface smoothing effects modify the surface/interface structure in multilayers. The results discussed in this paper are consistent with the idea that energetic-particle-induced smoothing during sputter deposition is the dominant effect in the WSi_2/Si bilayer system, and that very little ion beam mixing is introduced at the interfaces. The two effects are clearly distinguished by *in situ* measurements of roughness before and after the deposition of each layer.

II. EXPERIMENTS

The x-ray scattering measurements were performed at the National Synchrotron Light Source (NSLS) X21A station, where a monochromatic x-ray beam with 2×10^{12} photons/s flux is available through a Si (111) crystal monochromator. Synchrotron x rays with an energy of 10.4 keV ($\lambda=0.119$ nm) were employed to study thin film growth. For real-time *in situ* data collection, the experimental facility has integrated two subsystems for sample preparation and x-ray detection, respectively. An ultrahigh vacuum (UHV) chamber is used for thin film growth. The substrate is mounted on a custom-designed sample manipulator stage with horizontal surface normal. The manipulator fixed in the chamber has two orthogonal high-resolution rotation axes. Samples can make an in-plane rotation about the horizontal axis, and the whole manipulator stage can rotate about the vertical axis. The latter produces a rotation of the angle between the sample surface and the incident x-ray beam (α_i), as well as a rotation between the sample surface and the detector (α_f). Two beryllium windows in the UHV chamber allow the x-ray probe beam to enter and exit the chamber. The whole experiment including the chamber and the detector assembly rests on a table that can rotate about the vertical axis, which also affects α_i. The positions of the sample stage, detector, and the table were carefully aligned so that the sample surface and the detector were lined up with the incident x-ray beam before the deposition. Similar real-time UHV growth systems used at other synchrotron sources are described in other published reports.[12,25]

A linear position sensitive detector (PSD) was mounted on the detector arm in a vertical orientation. The linear detector has 320 pixels with 8 pixels/mm. The central 8 pixels of the PSD were set to always count the specular reflection intensity during all of the scans, which were done with $\alpha_i=\alpha_f$. Although off-specular intensities were recorded simultaneously with the specular ones during these measurements, we only report the specular intensity results in this paper. As described below, the PSD was replaced for certain measurements by a large dynamic range avalanche photodiode (APD) point detector.

The WSi_2 and Si films were deposited on superpolished silicon wafers by a dual-gun dc magnetron sputtering system with independently operating shutters. The substrate was kept at room temperature during the deposition. The dc sputtering power was 50 W for both WSi_2 and Si film depositions. During Si film deposition, the chamber was kept at 6×10^{-3} Torr argon pressure. For WSi_2 deposition, we chose two different argon pressures of 6×10^{-3} and 1.8×10^{-2} Torr to compare the effects of the pressure on the surface roughness. In order to investigate the possibility of energetic particle smoothing, ion beam sputtering was performed by a three-grid rf plasma ion source with an ion energy of 300 eV at a flux of 9×10^{14} ions/cm^2 s.

A series of x-ray scattering measurements were performed during deposition including real-time specular/off-specular intensity monitoring and *in situ* reflectivity scans after each deposited layer as follows: (1) For real-time film growth monitoring, both the grazing incidence angle α_i and the scattering angle α_f were set to 2.045°, corresponding to $Q_z=3.77$ nm^{-1}, by rotating the sample manipulator stage and the table. Real-time data, including both specular and off-specular intensities, were then collected with the PSD detector. (2) After the completion of each deposited layer, an *in situ* x-ray off-specular reflectivity scan for the deposited film was collected using the PSD. (3) The PSD was replaced with the APD point detector and the specular reflectivity scan was performed. Subsequently the whole process was repeated for the next WSi_2 or Si layer. The surface roughness and thickness of these films were derived from the specular x-ray reflectivity data using a least-squares fit, in which the reflected intensity is computed based on recursive application of the Fresnel equations.[26]

III. RESULTS AND DISCUSSION

A. Surface roughness evolution of WSi_2 and Si single layers

Figure 1 displays real-time specular reflectivity monitoring of a WSi_2 thin film grown at 6×10^{-3} Torr argon pressure. The film was deposited in three steps with individual (total) deposition times of 57 (57), 57 (114), and 119 (233) s, respectively. The reflectivity of the films show typical Kiessig fringes due to the interference of waves reflected from the top and bottom interfaces.[24] As can be seen in Fig. 1, the maxima of the reflection oscillations remain at almost a constant intensity level, indicating that under this argon pressure, the surface roughness does not change much as film thickness increases. The reflectivity oscillations also show that the growth interruption has no obvious influence on the film roughness.

In situ x-ray reflectivity results for two WSi_2 films deposited at different argon pressures are shown in Figs. 2(a) and 2(b), where the circles are the experimental data and the solid lines are simulations based on fits to the data. Curve 1

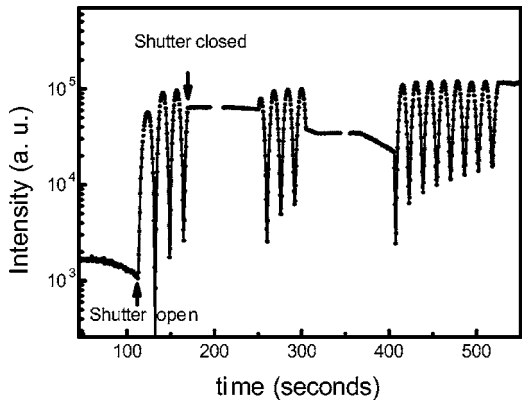

FIG. 1. Reflectivity of a WSi_2 film vs deposition time. The real-time monitoring for film growth was performed at $Q_z=3.77\ \text{nm}^{-1}$. The growth was interrupted twice in order to measure the reflectivity of the deposited film.

in Fig. 2(a) is the reflectivity of the Si substrate, while curves 2–4 show the reflectivity of WSi_2 films grown at 6×10^{-3} Torr with 57, 114, and 233 s total deposition times, respectively. Note that these data are for the same film shown in Fig. 1. Figure 2(b) presents the reflectivity data of WSi_2 deposited at 1.8×10^{-2} Torr argon pressure. Curves 1–3 correspond to total deposition times of 45, 90, and 180 s, respectively. The reflectivity oscillations damp out quickly with increasing incident angle and film thickness, indicating a rapid increase in surface roughness compared to the data shown in Fig. 2(a).

The simulations of the reflectivity curves along with fitting results from the IMD software package are plotted as solid lines in Figs. 2(a) and 2(b). From the thickness values displayed in Table I, the WSi_2 deposition rates are 0.096 nm/s for deposition at 6×10^{-3} Torr and 0.135 nm/s at 1.8×10^{-2} Torr. As shown in Table I, the surface roughness depends on the deposition pressure: For the WSi_2 thin film grown at 6×10^{-3} Torr argon pressure, the surface roughness increases to $\sigma_{\text{film}}=0.32$ nm at the final thickness of $d=22.4$ nm. However, the WSi_2 film prepared at 1.8×10^{-2} Torr is much rougher; the surface roughness is $\sigma_{\text{film}}=1.53$ nm at $d=24.4$ nm, almost five times larger than the corresponding value at the lower argon pressure.

Figure 2(c) shows the reflectivity of a Si film deposited at 6×10^{-3} Torr, in which curves 1–3 correspond to 93, 186, and 372 s total deposition times. The simulated roughness and thickness results are also listed in Table I. The deposition rate is found to be 0.060 nm/s. The oscillations in these curves are also damped at higher angles, which indicates the presence of significant surface roughness on the Si film. The Si film is much rougher than the WSi_2 film deposited at the same pressure, although it is smoother than the WSi_2 film deposited at the higher pressure.

B. Roughness evolution in WSi_2/Si multilayers

An initial investigation of interface roughness evolution in WSi_2/Si multilayers was performed by depositing a bilayer structure. A 6 nm thick WSi_2 layer was deposited onto the Si film originally presented in Fig. 2(c). This was done immediately after the Si deposition, so that there was minimal contamination of the Si surface. Both layers were deposited at 6×10^{-3} Torr argon pressure. In Fig. 3, the part of the curve before the break shows the real-time x-ray reflection intensity during the final part of the Si deposition. It is clearly seen that the intensity oscillations are quickly damped due to the rapid surface roughness increase. However, during the subsequent WSi_2 layer deposition, the real-time x-ray intensity oscillations display a different character, which is shown in the right part of Fig. 3. The reflected intensity rises quickly and the oscillation amplitude increases

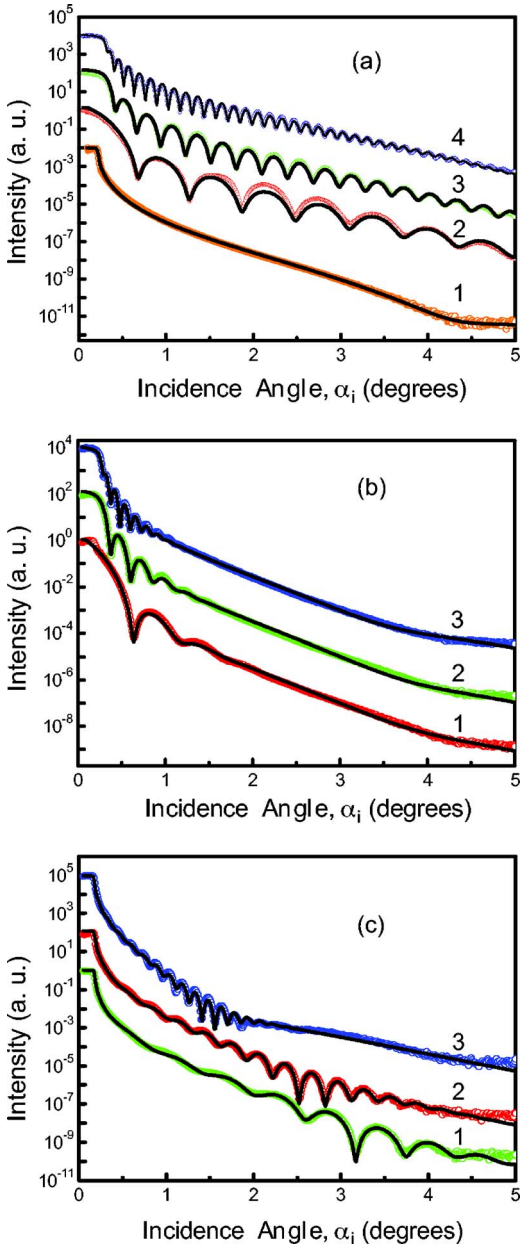

FIG. 2. Normalized x-ray reflectivity measured in WSi_2 and Si films, where the circles are the experimental data and the solid lines represent the fitting results. For clarity, the curves are shifted vertically. (a) is the reflectivity of the WSi_2 films grown at 6×10^{-3} Torr pressure. Curve 1 is the reflectivity of the bare Si substrate, while curves 2–4 correspond to reflectivity of a WSi_2 layer with total deposition times of 57, 114, and 233 s, respectively. (b) presents the reflectivity data of WSi_2 film deposited at 1.8×10^{-2} Torr argon pressure. Curves 1–3 are for total deposition times of 45, 90, and 180 s, respectively. (c) shows the reflectivity of a Si film deposited at 6×10^{-3} Torr, in which 1–3 correspond to 93, 186, 372 s total deposition times.

TABLE I. The thickness (d) and surface roughness (σ) results of WSi_2 and Si films deposited at different argon pressures.

Sample	Deposition time (s)	Thickness (nm)	Roughness (nm)
Si substrate	···	SiO_2: 0.43	SiO_2/Si interface: 0.17 SiO_2 surface: 0.25
WSi_2 film deposited at 6×10^{-3} Torr	57	5.5	0.21
	114	11.5	0.22
	233	22.4	0.32
WSi_2 film deposited at 1.8×10^{-2} Torr	45	5.8	0.94
	90	12.3	1.23
	180	24.4	1.53
Si films deposited at 6×10^{-3} Torr	93	5.5	0.38
	186	11.0	0.46
	372	22.5	0.82

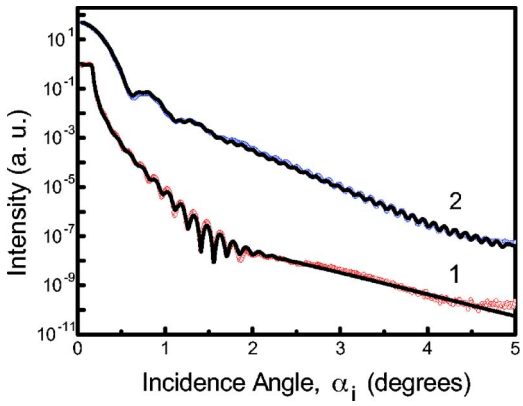

FIG. 4. X-ray reflectivity data of a WSi_2/Si bilayer. Curve 1 is the reflectivity data after the deposition of the Si layer underneath, while curve 2 is the reflectivity after the deposition of the WSi_2 top layer. The open circles and the solid lines represent experimental data and fitting results, respectively.

with the deposition time. We interpret the initial large increase of the intensity as being due to the larger electron density of WSi_2 layer, while the more gradual increase in the oscillation amplitude implies that the surface roughness decreases during film deposition.

The x-ray reflectivity results from this WSi_2/Si bilayer are presented in Fig. 4. The reflectivity of the initial Si film presented in Fig. 2(c) curve 3 is now redrawn as curve 1 in Fig. 4, while curve 2 is the reflectivity after the WSi_2 deposition. Comparing the two reflectivity curves, it can be seen that the oscillations appear again at higher incident angles in the reflectivity curve of the WSi_2/Si bilayer. The fitting results from curve 2 reveal that the surface roughness of the top WSi_2 layer is σ=0.33 nm and the thickness is d=6.2 nm, while the interface roughness between the WSi_2 and Si layers is 0.74 nm and the thickness of Si layer is 22.4 nm. These results show that the upper WSi_2 layer has a smoother surface than the Si layer underneath it, suggesting that the high-frequency surface roughness initially present on the Si surface is gradually smoothed out on the WSi_2 growth surface due to the strong smoothing mechanism taking place in the WSi_2 deposition process.

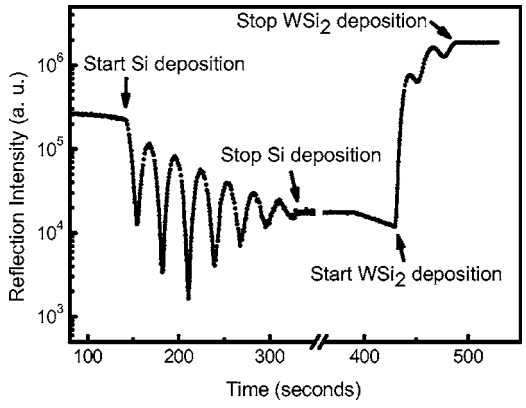

FIG. 3. Real-time x-ray reflection intensity oscillations observed during the growth of a Si layer and the following WSi_2 layer. The intensity oscillations are quickly damped out during the deposition of the Si layer, but recover again when the WSi_2 layer is deposited.

Another notable effect that is apparent in the fitting results of the data shown in Fig. 4 is the change of the roughness of the initial Si layer before and after WSi_2 deposition. As mentioned above for curve 2 in Fig. 4, the interface roughness between WSi_2 and Si is 0.74 nm. This can be compared to the roughness value for the Si layer before the overgrowth of the WSi_2 layer, 0.82 nm, as listed in Table I, which suggests that the Si surface is actually smoothed slightly during the overgrowth process. This is contrary to the expectation that energetic particles induce interface mixing, and suggests that, instead, energetic particles sputtered/reflected from the WSi_2 target may impact and smoothen the Si surface through the same smoothing mechanism as occurred in the WSi_2 layer deposition. Presumably, this process takes place only during the very early part of the WSi_2 deposition before the surface of the Si layer is completely covered.

To verify the smoothing effect produced by ion bombardment, we used an ion beam with 300 eV energy to etch a rough Si film. The real-time x-ray intensity monitoring for the ion polishing process is displayed in Fig. 5. It demonstrates that the intensity oscillations gradually increase with etching time. Note that the initial large increase in intensity

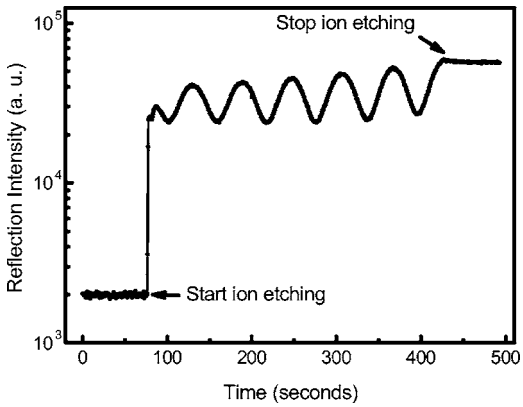

FIG. 5. Real-time x-ray reflectivity monitoring for etching of a Si film. The increase in oscillation amplitude shows that ion polishing effectively smoothes the Si surface.

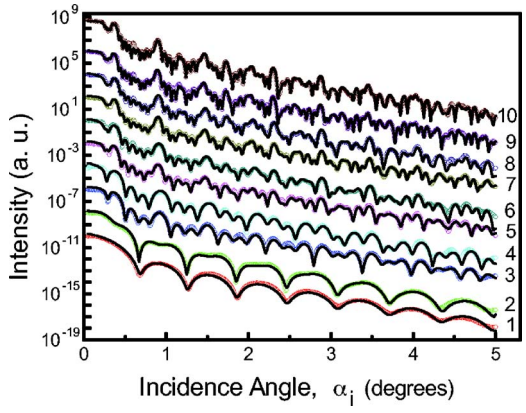

FIG. 6. *In situ* x-ray reflectivity after each layer of the deposition of a WSi_2/Si multilayer. The numbers in the figure correspond to the numbers of layers at each stage.

is due to the removal of water vapor from the surface, since this particular sample was exposed to air prior to the etching experiment. According to the fitting results from the x-ray reflectivity of the Si film before and after ion polishing (the x-ray reflectivity curves are not shown), the Si film is 23.1 nm thick with 0.66 nm surface roughness before the ion polishing. After 343 s etching, the thickness and surface roughness of the Si film are reduced to 12.7 and 0.23 nm, respectively.

Finally, we deposited a WSi_2/Si multilayer structure with five periods at 6×10^{-3} Torr argon pressure. After each layer deposition, the x-ray reflectivity of the sample was measured and the ten curves are plotted in Fig. 6. The numeric labels for each curve correspond to the topmost layer in the multilayer at that stage of the deposition. The circles represent the experimental data and the solid lines display the fitting results. In modeling these data, we have assumed that the topmost layer deposited at any time modifies only the layer directly underneath it. Therefore, when fitting one curve, only the parameters of the top two layers were allowed to vary, while the parameters of the deeper buried layers were fixed at values that had been determined in the previous fitting steps. Table II lists both roughness results for each layer: a surface roughness and an interface roughness determined after deposition of the next layer.

TABLE II. The thickness and roughness results for a WSi_2/Si multilayer with five periods.

Layer	Thickness (nm)	Roughness (nm) (as surface)	Roughness (nm) (as interface)
a-Si layer (tenth layer)	6.0	0.39	···
WSi_2 layer (ninth layer)	6.4	0.24	0.26
a-Si layer (eighth layer)	5.7	0.37	0.35
WSi_2 layer (seventh layer)	6.3	0.23	0.27
a-Si layer (sixth layer)	5.5	0.36	0.38
WSi_2 layer (fifth layer)	6.4	0.22	0.25
a-Si layer (fourth layer)	5.6	0.38	0.35
WSi_2 layer (third layer)	6.2	0.23	0.27
a-Si layer (second layer)	5.4	0.41	0.40
WSi_2 layer (first layer)	5.5	0.24	0.27
SiO_2 layer	0.5	0.25	0.26
Si substrate	···	···	0.17

According to the fitting result, the structure of the WSi_2/Si multilayer shows an alternating smooth and rough interface. The interfaces with Si on WSi_2 are smoother than the interfaces with WSi_2 on Si. Though this asymmetrical interface structure has been reported in other multilayer systems,[6,15] the formation mechanism of the asymmetrical structure in WSi_2/Si multilayers is different than what was previously reported. Usually, a ballistic argument has been proposed to interpret the asymmetry. It is believed that the heavy atoms will easily penetrate into the surface when these atoms impinge on the light-atom layer, producing an intermixed interface as compared to the light-on-heavy interface.[6] In our observations, the WSi_2 layer deposition does not increase the roughness of Si layer. From the above discussion of the roughness evolution of WSi_2 and Si single layers and WSi_2/Si bilayers, we argue that the interface roughness asymmetry originates only from the smoothing mechanism taking place in the thin film deposition process. Because there is a stronger smoothing effect during the WSi_2 layer growth, the surface roughness of Si is intrinsically larger than the surface roughness of the WSi_2 layer at the same deposition parameters. When WSi_2 is deposited on a rough Si layer, the initial roughness of the Si layer is damped out so that the WSi_2 has a smoother surface, resulting in an asymmetrical interface roughness. The fitting results also indicate that the accumulated roughness in this multilayer structure is very small. The total roughness does not show much of an increase with the number of periods because the smoothing process effectively prevents the accumulation of roughness.

IV. CONCLUSIONS

We have observed interface roughness evolution in sputtered WSi_2/Si single layers and multilayers by *in situ* synchrotron x-ray scattering. The surface roughness increases very slowly in the WSi_2 layer when deposited at a low argon pressure of 6×10^{-3} Torr due to a strong smoothing mechanism probably induced by the energetic flux. When a WSi_2 layer is deposited on a rough Si layer at the optimized background argon pressure, the WSi_2 layer is rapidly smoothed, but the buried Si layer remains rough. This mechanism is believed to be responsible for the asymmetrical interface roughness in the WSi_2/Si multilayers. No evidence for the ion beam mixing effect has been observed.

ACKNOWLEDGMENTS

The facility for real-time x-ray studies of surface processes was funded by the National Science Foundation under Grant No. DMR-0216704. This work was financially supported by the Office of Basic Energy Sciences of the U.S. Department of Energy through Grant No. DE-FG02-03ER46032 and by the NSF through DMR-0216704. The authors also gratefully acknowledge the support of Lin Yang, Chi-Chang Kao, D. Peter Siddons, and Wolfgang A. Caliebe at the NSLS who helped make the x-ray experiments on beamline X21 possible. Financial support for NSLS comes principally from the Office of Biological and Environmental

Research and of Basic Energy Sciences of the U.S. Department of Energy.

[1]A. Patelli, J. Ravagnan, V. Rigato, G. Salmaso, D. Silvestrini, E. Bontempi, and L. E. Depero, Appl. Surf. Sci. **238**, 262 (2004).
[2]J. Birch, F. Eriksson, G. A. Johansson, and H. M. Hertz, Vacuum **68**, 275 (2003).
[3]D. G. Stearns and E. M. Gullikson, Physica B **283**, 84 (2000).
[4]D. L. Windt, R. Hull, and W. K. Waskiewicz, J. Appl. Phys. **71**, 2675 (1992).
[5]D. G. Stearns, M. B. Stearns, Y. Cheng, J. H. Stith, and N. M. Ceglio, J. Appl. Phys. **67**, 2415 (1990).
[6]A. K. Petford-Long, M. B. Stearns, C. H. Chang, S. R. Nutt, D. G. Stearns, N. M. Ceglio, and A. M. Hawryluk, J. Appl. Phys. **61**, 1422 (1987).
[7]C. Liu, R. Conley, A. Macrander, J. Maser, H. Kang, M. Zurbuchen, and G. Stephenson, J. Appl. Phys. **98**, 113519 (2005).
[8]H. Kang, J. Maser, G. Stephenson, C. Liu, R. Conley, A. Macrander, and S. Vogt, Phys. Rev. Lett. **96**, 127401 (2006).
[9]A.-L. Barabási and H. E. Stanley, *Fractal Concepts in Surface Growth* (Cambridge University Press, Cambridge, England, 1995).
[10]Z. Zhang and M. G. Lagally, Science **276**, 377 (1997).
[11]A. T. Macrander, C. Liu, R. Csencsits, R. Cook, M. Kirk, and R. Headrick, Physica B **283**, 157 (2000).
[12]L. Peverini, E. Ziegler, T. Bigault, and I. Kozhevnikov, Phys. Rev. B **72**, 045445 (2005).
[13]M. Moseler, P. Gumbsch, C. Casiraghi, A. C. Ferrari, and J. Robertson, Science **309**, 1545 (2005).
[14]C. Casiraghi, A. C. Ferrari, R. Ohr, A. J. Flewitt, D. P. Chu, and J. Robertson, Phys. Rev. Lett. **91**, 226104 (2003).
[15]Z.-J. Liu and Y. G. Shen, Appl. Phys. Lett. **84**, 5121 (2004).
[16]R. Schlatmann, J. D. Shindler, and J. Verhoeven, Phys. Rev. B **54**, 10880 (1996).
[17]F. Family, J. Phys. A **18**, L75 (1985).
[18]S. D. Sarma and P. Tamborenea, Phys. Rev. Lett. **66**, 325 (1991).
[19]C. C. Umbach, R. L. Headrick, and K.-C. Chang, Phys. Rev. Lett. **87**, 246104 (2001).
[20]K. Oyoshi, T. Tagami, and S. Tanaka, Jpn. J. Appl. Phys., Part 1 **30**, 1854 (1991).
[21]V. Rigato *et al.*, Surf. Coat. Technol. **174–175**, 40 (2003).
[22]E. Spiller, Appl. Phys. Lett. **54**, 2293 (1989).
[23]B. Window, J. Vac. Sci. Technol. A **11**, 1522 (1993).
[24]J. A. Nielsen and D. McMorrow, *Elements of Modern X-ray Physics* (Wiley, England, 2001).
[25]R. L. Headrick, S. Kycia, Y. K. Park, A. R. Woll, and J. D. Brock, Phys. Rev. B **54**, 14686 (1996).
[26]D. L. Windt, Comput. Phys. **12**, 360 (1998).